New Wrinkles in Retinal Densitometry

Benjamin D. Masella,[1,2] Jennifer J. Hunter,[2,3] and David R. Williams[1–3]

[1]The Institute of Optics, University of Rochester, Rochester, New York, United States
[2]Center for Visual Science, University of Rochester, Rochester, New York, United States
[3]Flaum Eye Institute, University of Rochester, Rochester, New York, United States

Correspondence: Benjamin D. Masella, 55 Black Brook Road, Keene, NH 03431, USA; bmasella@cvs.rochester.edu.

Submitted: December 18, 2013
Accepted: September 30, 2014

Citation: Masella BD, Hunter JJ, Williams DR. New wrinkles in retinal densitometry. *Invest Ophthalmol Vis Sci*. 2014;55:7525–7534. DOI: 10.1167/iovs.13-13795

Purpose. Retinal densitometry provides objective information about retinal function. But, a number of factors, including retinal reflectance changes that are not directly related to photopigment depletion, complicate its interpretation. We explore these factors and suggest a method to minimize their impact.

Methods. An adaptive optics scanning light ophthalmoscope (AOSLO) was used to measure changes in photoreceptor reflectance in monkeys before and after photopigment bleaching with 514-nm light. Reflectance measurements at 514 nm and 794 nm were recorded simultaneously. Several methods of normalization to extract the apparent optical density of the photopigment were compared.

Results. We identified stimulus-related fluctuations in 794-nm reflectance that are not associated with photopigment absorptance and occur in both rods and cones. These changes had a magnitude approaching those associated directly with pigment depletion, precluding the use of infrared reflectance for normalization. We used a spatial normalization method instead, which avoided the fluctuations in the near infrared, as well as a confocal AOSLO designed to minimize light from layers other than the receptors. However, these methods produced a surprisingly low estimate of the apparent rhodopsin density (animal 1: 0.073 $\pm$ 0.006, animal 2: 0.032 $\pm$ 0.003).

Conclusions. These results confirm earlier observations that changes in photopigment absorption are not the only source of retinal reflectance change during dark adaptation. It appears that the stray light that has historically reduced the apparent density of cone photopigment in retinal densitometry arises predominantly from layers near the photoreceptors themselves. Despite these complications, this method provides a valuable, objective measure of retinal function.

Keywords: dark adaptation, densitometry, intrinsic signals, adaptive optics, rhodopsin regeneration

The recovery of the visual system after exposure to bright adapting lights provides insight into retinal function in health and disease.[1–15] Retinal densitometry is an attractive method for tracking this recovery because, unlike psychophysical approaches, it is objective. Typically, retinal reflectance is measured at a wavelength that is highly absorbed by visual pigment. Comparison of the measured reflectance in the dark-adapted (or partially dark-adapted) state to that in the bleached state is used to calculate the pigment optical density. It has long been known that stray light, which is difficult to measure, complicates estimation of the true pigment density from reflectance measurements.[8,16,17] Nonetheless, it was thought that changes in retinal reflectance after exposure to bright light were entirely attributable to changes in photopigment density. Indeed, the widely accepted method to reject changes not related to the photopigment has been to normalize reflectance changes in the visible with those in the infrared under the assumption that the only difference between the infrared and visible reflectances is due to photopigment absorption. However, DeLint et al.[18] found significant, non–photopigment-related fluctuations in retinal reflectance that further complicate the interpretation of retinal densitometry and result in an overestimate of the density of the photopigment. Specifically, they discovered slow changes in infrared reflectance near the fovea that were attributable to cone photoreceptors, but that could not be explained by changes in photopigment absorptance.

Our goal was to incorporate objective measures of retinal function, such as retinal densitometry, into modern ophthalmoscopes that provide cellular-resolution imaging of retinal structure in the living eye. A number of researchers have already combined retinal densitometry with adaptive optics ophthalmoscopes for the study of cone photoreceptors. Roorda and Williams[15] demonstrated that reflectance changes after photopigment bleaches at different wavelengths could be used to identify the type of each cone in a small area of retina. In 2012, Bedggood and Metha[19] were able to measure the time course of photopigment bleaching in individual cones using a similar method. We developed an instrument that tracks the function of the rod photoreceptors using retinal densitometry at high spatial resolution. The instrument can provide reliable measurements of the reflectance changes after bleaching while resolving photoreceptors. With this device, we have discovered effects in rod photoreceptors similar to those described by DeLint et al.[18] in cones, that further challenge the simple

Table 1. Information About the Two Animals, Their Eyes, and Contact Lenses Used During All Retinal Imaging Experiments

Animal	1	2
Species	*Macaca mulatta*	*Macaca fascicularis*
Sex	Female	Male
Age, y	14	19
Eye imaged	OD (right)	OD (right)
Axial length of imaged eye, mm	20.6 ± 0.10	19.0 ± 0.14
Corneal radius of curvature, mm*	6.35 ± 0.50	5.70 ± 0.07
Contact lens base radius of curvature, mm	6.25	5.95
Contact lens diameter, mm	10.0	12.2
Contact lens power, D	−3	−3

* Radius of curvature reported is the mean of the measured vertical and horizontal radii.

photopigment-absorptance interpretation of retinal densitometry.

Methods

Nonhuman Primates

The in vivo experiments in this study were performed using two macaque monkeys and were approved by The University of Rochester's Committee on Animal Resources and adhere to the ARVO Statement for the use of Animals in Ophthalmic and Vision Research. Specific information about the individual primates used is shown in Table 1. Before each imaging experiment, the animal was injected with ketamine (18–21.5 mg/kg), glycopyrrolate (0.017 mg/kg), ketofen (5 mg/kg), and, when available, valium (0.25 mg/kg). During experiments, the monkeys were anesthetized with isoflurane gas (1.0%–3.0%), paralyzed with vecuronium bromide (1 mg/kg bolus, followed by 60 μg/kg/h), and their pupils dilated and cyclopleged with 1 to 2 drops each of phenylephrine hydrochloride (2.5%) and tropicamide (1%). A lid speculum was used to hold the eye open and a hard contact lens protected the cornea and corrected some refractive error. A head post, gimbal mount, and three-axis stage were used to align the animal's head and pupil with the imaging system and allow for stable control of retinal image location.[20]

Apparatus

The optical system was a custom-built adaptive optics scanning light ophthalmoscope (AOSLO) with two imaging channels, the design of which has been published previously.[21] This system scans a point of light in a raster pattern using two galvanometer-driven scanning mirrors. The monochromatic aberrations of the eye were measured using an 850-nm laser diode and a Shack-Hartmann wavefront sensor. Closed-loop wavefront correction was performed using a 97 actuator deformable mirror (ALPAO DM97-15; ALPAO, Biviers, France). The system's two imaging channels were separated by a long-pass dichroic filter (cutoff: 750 nm), allowing reflectance imaging of two sources simultaneously: a superluminescent diode (SLD; 794 nm Δ17 nm), and an argon/krypton (ArKr) gas laser tuned to 514 nm. Light directed to each channel was focused through a pinhole of two Airy disks in diameter and detected by a photomultiplier tube, the sensitivity of which was chosen to match each source (Hamamatsu [Hamamatsu, Japan] H7422-40 for visible, −50 for NIR). Because accurate radiometry was required, the optical system was isolated with a light-tight box and the animal's head was covered with opaque fabric.

Procedure

Using NIR reflectance only, a retinal location was first chosen that had minimal retinal vasculature and lay near the peak density of the rod photoreceptors (∼15° from the fovea). The animal was then dark adapted for 60 minutes, after which pairs of 2-second videos were recorded simultaneously, one at 514 nm and the other at 794 nm. The first video captured the retinal reflectance before photopigment bleaching, the second occurred during the bleach, and subsequent videos tracked the reflectance changes during 35 minutes of dark adaptation. These videos were recorded at 0, 2.5, 5.0, 7.5, 10.0, 15.0, 20.0, 25.0, 30.0, and 35.0 minutes after the bleach. Each video corresponded to a square 2° × 2° retinal region. The rhodopsin bleaching exposure (ArKr, 514 nm) was limited to a one-third degree by one-half degree rectangular region at the center of the 2° AOSLO raster scan. This was achieved by modulating the 514-nm laser intensity with an acousto-optic modulator (AOM; Brimrose [Sparks Glencoe, MD, USA] model TEM-200-50-485/635-02FP attached with an OZ-Optics [Ottawa, ON, Canada] fiber coupler model HPUC-2A3A-400/700-P-4.5AC-15) set to maximum transmission in the central region to be bleached and zero elsewhere.

Using this method, the time course of dark adaptation was measured four times in each of eight retinal locations in one eye of each primate, for a total of 64 bleach and recovery measurements.

Photopigment Bleaching

The effect of the bleaching exposure was measured experimentally by dark adapting the retina and using the AOSLO to record 514-nm reflectance videos at an average power of 11.4 μW. After repeating this in four retinal locations in animal 1, the average reflectance measured over time was calculated and fit to equation (3) from Morgan and Pugh,[14] shown below as equation (1).

$$p(t) = e^{-\left(\frac{Q}{Q_e}\right)} \quad (1)$$

Here, p is the fraction of pigment remaining at time t seconds, Q is retinal luminous exposure in Td·s (i.e., the product of retinal illuminance and exposure duration), Q_e is the photosensitivity of rhodopsin bleaching in vivo, which is the energy (in Td·s) needed to bleach p from 1 to e^{-1}.

Bleaching From All Light Sources Used in Recovery Experiments

To measure the density of rhodopsin without perturbing it, we chose to limit the irradiance and duration of our measurements such that the total retinal radiant exposure for a single measurement would cause less than a 1% change in unbleached rhodopsin density. Two seconds of AOSLO reflectance imaging at 514 nm, with an average power of 50 nW at the cornea and a 2° × 2° raster scan, was determined to provide sufficient signal-to-noise (SNR) for our measurements. The scotopic energy density for this measurement was 1.7×10^5 scot Td·s. All postbleach density measurements were separated by at least 2.5 minutes to limit any cumulative effect on rhodopsin density.

Because of the limited extinction ratio of the AOM (∼100:1), the area of the retina over which the AOM was in its off state was exposed to 200 nW of 514-nm power during an average 2-second bleaching exposure. This would cause a 3%

reduction of rhodopsin concentration in the retinal region intended for normalization of the density measurements. Initial rhodopsin recovery rates for human subjects have been previously reported to be approximately 9% per minute.[22] Therefore, the rhodopsin concentration in the region used for normalization will be greater than 99% of its dark-adapted value by the second density measurement at 2.5 minutes. To minimize the light-adapting effect of the 514-nm measuring beam, a mechanical shutter blocked the output from this source between measurements.

The 850-nm wavefront-sensing source was set to an average power of 20 μW at the cornea for every experiment. This source remained on continuously to allow closed-loop operation of the adaptive optics system. No retinal location was imaged continuously for more than 50 minutes, giving a maximum possible scotopic energy density of 3.0×10^2 scot Td·s from this source. This would bleach 3.0×10^{-4}% of available rhodopsin; therefore, the effect of this source on rhodopsin density was ignored.

The maximum 794-nm SLD power at the pupil of the eye was 350 μW. This setting was used for initial alignment of the retinal location to be bleached and during the recording of the first three videos: prebleach, bleach, and postbleach. The maximum exposure time for each retinal location at this power was 2 minutes, corresponding to a maximum scotopic energy density of 1.6×10^4 scot Td·s. During the remaining imaging time at each location, the SLD power was reduced to 20 μW, which produced a negligible energy density compared with the initial 2 minutes. Thus, the total scotopic energy density from this source was 1.6×10^4 scot Td·s, which would bleach less than 0.06% of available rhodopsin. Once again, the effect of this source on rhodopsin density is negligible and was ignored.

Postprocessing

The data recorded at each time point for a given rhodopsin recovery measurement consisted of two simultaneous 8-bit AVI videos, one at 794 nm and one at 514 nm, with 48 usable frames each. Because of the low SNR of the 514 nm measurement, all 48 frames were registered and averaged to generate a single retinal image from each video. A dual-image registration and averaging method, in which the high-SNR 794-nm videos were used to calculate and correct for eye movements in both channels, was used to generate a series of 12 uncompressed, 8-bit TIFF images from each channel, corresponding to the bleach and rhodopsin measurements. This registration method has been reported previously[23–26] and made use of software developed by Dubra and Harvey.[26]

Once these TIFF images were generated, additional custom software written using Mathworks Matlab (Natick, MA, USA) was used to calculate average pixel intensities. First, the 514-nm image corresponding to the bleaching exposure was used to identify the retinal area that had been bleached. Then this region was cross-correlated with the simultaneously acquired 794-nm image to measure any shift caused by either minor noncommon path misalignments or transverse chromatic aberration. Once the bleach coordinates and the shift between the two channels had been determined, each 794-nm image (excluding the bleaching exposure) was cross-correlated with the prebleach image to determine the drift in retinal position at each time point. Each image was then cropped such that all 794-nm and 514-nm images contained the same retinal area.

Once all images were aligned and cropped, their average reflectance could be compared. The mean pixel values inside and outside the bleached region were calculated for each of the 514-nm images. A margin of 10 pixels surrounding the bleached region was excluded to prevent small retinal movements from affecting the measurement. These values also were calculated for the 794-nm images.

Relating Retinal Reflectance Changes to Pigment Density

As mentioned earlier, uncertainty about the amount of light that does not pass through photopigment has been a problem in estimating true photopigment density from reflectance measurements because this light dilutes the reflectance changes caused by pigment regeneration. A possible advantage of performing densitometry measurements with an AOSLO is that the contribution of stray light is greatly reduced. The model of fundus reflectance proposed by van de Kraats et al.[27] is appropriate for the case of an SLO. This model separates retinal fundus reflectance into that originating anterior to the photoreceptors (e.g., cornea, lens, vitreous), that from the photoreceptors, and that beyond the photoreceptors (RPE, choroid, sclera). This model was summarized by Morgan and Pugh[14] with the following equation:

$$R_{eye}(\lambda) = \tau_\lambda^2 \left\{ R_{prePR} + \left[1 - R_{prePR}\right]^2 \left[R_{PR}(\lambda) + R_{postPR}(\lambda)\right] \right\}. \quad (2)$$

In this equation, τ_λ is the transmissivity anterior to the photoreceptors, R_{prePR} is the reflectance of ocular structures anterior to the photoreceptors, R_{PR} is the reflectance of the photoreceptors, and R_{postPR} is the reflectance posterior to the photoreceptors.

However, this equation can be greatly simplified in the case of the AOSLO, because the confocal pinhole in the detection channel significantly reduces the contribution of pre- and post-photoreceptor reflectance to the measured signal. Assuming diffraction-limited performance of the AO system, the theoretical full width at half maximum of the axial intensity response of the AOSLO used in this study was 60 μm at 514 nm.[28] Because all measurements were taken with the AOSLO focused at the photoreceptor layer, equation (2) can be simplified to

$$R_{measured}(514) = \tau_{514}^2 [R_{PR}(514)]. \quad (3)$$

Although the high axial resolution of the AOSLO reduces stray light, for example, from the inner retina, some fraction of the reflected light will have scattered from the inner segments, passed between the photoreceptors, or passed through only a portion of the outer segment. This is why the term apparent density has been chosen, as this value does not represent the real absolute density of rhodopsin in the outer segments.

Also, confocality does not reject reflectance changes other than those caused by photopigment absorptance, such as might arise in the instrument or other optical changes in or near the receptors. We compared three different normalization methods to remove these unwanted variations in reflectance: infrared, spatial, and a combination of the two.

Using the infrared normalization method, we defined the apparent optical density of rhodopsin with the following equation:

$$D_{apparent} = log_{10}\left[\frac{R_{514,b}}{R_{794,b}} / \frac{R_{514,d}}{R_{794,d}}\right], \quad (4)$$

where R_{514} and R_{794} represent the simultaneous reflectance measured at each wavelength within the bleached region, and the subscripts b and d indicate measurements taken in the bleached and dark-adapted states, respectively. This method of reflectance normalization has been used many times previously.[3,6,8]

The spatial approach uses the surrounding dark-adapted area of the 514 nm AOSLO images to normalize the rhodopsin

density measurements. The apparent density measurement in this case is given by

$$D_{apparent} = log_{10}\left[\frac{R_{in,b}}{R_{out,b}} / \frac{R_{in,d}}{R_{out,d}}\right], \quad (5)$$

where R_{in} and R_{out} represent the 514-nm reflectance measured inside and outside the bleached region of the image, respectively, and the subscripts b and d again indicate measurements taken in the bleached and dark-adapted states.

Finally, we tested a combined method in which we first take the ratio of the bleached to the surrounding dark-adapted area at each wavelength and then normalize the 514-nm ratio to that at 794 nm. This is very similar to the reflectance double ratio described by Morgan and Pugh.[14] This measure is given by the equation

$$D_{apparent} = log_{10}\left[\left(\frac{R_{514,in,b}/R_{514,out,b}}{R_{794,in,b}/R_{794,out,b}}\right) / \left(\frac{R_{514,in,d}/R_{514,out,d}}{R_{794,in,d}/R_{794,out,d}}\right)\right]. \quad (6)$$

In previous studies, both the reflectance at 794 nm and that from the unbleached outside area are assumed to remain constant between the pre- and immediate postbleach conditions, in which case equations (4), (5), and (6) all simplify to

$$D_{apparent} = log_{10}\left[\frac{R_{514,in,b}}{R_{514,in,d}}\right]. \quad (7)$$

By combining equations (3) and (7), regardless of the normalization technique, apparent density has no dependence on pre-photoreceptor transmissivity:

$$D_{apparent} = log_{10}\left[\frac{R_{PR,b}}{R_{PR,d}}\right]. \quad (8)$$

However, this assumes that transmissivity is constant during all measurements following a given bleaching exposure, an assumption we will later directly challenge.

Fitting the Rhodopsin Recovery Time Course

The time course of rhodopsin recovery was assumed to follow rate-limited recovery kinetics as described by Mahroo and Lamb in 2004.[29] The average apparent rhodopsin density over time of the four recovery measurements taken in each retinal location was fit using this equation:

$$D(t) = D_{apparent} \cdot K_m \cdot W\left\{\left(\frac{B}{K_m}\right) e^{\left(\frac{B}{K_m}\right)} e^{-\left(\frac{1-K_m}{K_m}\right)vt}\right\}, \quad (9)$$

where, $D(t)$ is the instantaneous apparent density, $D_{apparent}$ is the effective dark-adapted rhodopsin density, and B is the fraction of rhodopsin bleached. K_m is analogous to the Michaelis constant in enzyme kinetics.[30] The variable v is the initial rate of rhodopsin recovery, t is time from the bleach, and W is the Lambert W function.

When fitting the regeneration time course, the data point immediately following the bleach ($t = 0$) was excluded because, as previously mentioned, the normalization region was partially bleached at that time, but was assumed to be fully dark adapted from 2.5 minutes after bleach. To calculate the value of K_m, all 64 data sets were averaged together and fit using the rate-limited model. The best fit for K_m was found to be 0.2. This value was then fixed when determining the best-fit values for $D_{apparent}$ and v for individual retinal locations.

By approximately 20 minutes after the bleach, retinal reflectance had decreased to a value that on average was approximately 1% greater than the prebleach measurement. When calculating the dark-adapted reflectance values, the mean of the last four measurements (20–35 minutes post-bleach) was used.

Separation of Rod and Cone Reflectance

At one location in animal 1, we relied on the high spatial resolution of the AOSLO to remove cone reflectance changes from those generated by rods. Adobe Photoshop (Adobe Systems, Inc., San Jose, CA, USA) was used to manually identify the center pixel of each cone within the bleached area of the AOSLO images collected for eight bleaches. A mask was then generated to identify all cone-related pixels in each image by modeling each cone as a normalized Gaussian intensity distribution with full width at half maximum equal to a third of the average distance to its nearest neighbors. This modeled image was then converted to a binary mask with every pixel below 20% of the maximum set to zero. This mask excluded much of the light returning from cones. Its inverse was used to exclude much of the light returning from rods. Photopigment densities and recovery rates were then determined and compared for the rods and cones in combination and the rods separately. Measured NIR reflectance changes of rods and cones were also compared. Low SNR of the 514-nm measurements rendered cone-only densitometry data unreliable.

Results

Photopigment Bleaching

During bleaching, the 514-nm reflectance intensity of the exposed region increased, corresponding to a decrease in photopigment density. The mean of the measured data from four test bleaches in four different locations in animal 1 is shown in Figure 1. A least-squares fit of the average of the four test bleaches to Equation 1 produced a mean value for the photosensitivity (Q_e) of rhodopsin bleaching in the primate retina of 7.2 ± 1.2 log Td·s. This is consistent with values previously reported in the human eye.[14]

Reflectance Changes With Bleaching

Figure 2 shows localized changes in retinal reflectance at 514 nm and 794 nm immediately following a photopigment bleach. Cones are visible in the images but rods are not, largely because we were limited to 480 raster lines per image over a 2-degree scan, resulting in approximately 2 μm per sample, which is inadequate to resolve individual rods. This choice of field size sacrificed rod resolution for increased imaging area and improved signal-to-noise for the density measurements, because a larger scanning field allowed for higher average 514-nm power through the pupil without increasing average irradiance at the retina.

At 514 nm, the retinal reflectance increases immediately after the bleach and then decreases back to baseline as photopigment regenerates. Reflectance images at 794 nm showed systematic oscillations in NIR reflectance in response to bleaching exposures. Figure 3 quantifies these oscillations, showing the mean 794-nm reflectance ratio (inside/outside the bleached area) as a function of time from bleach, normalized to the prebleach condition for both animals and the mean. Despite individual differences in magnitude, both animals showed an immediate drop in relative NIR reflectance followed by an increase that overshoots the baseline. This increase peaks at approximately 7.5 minutes after the bleach. The reflectance then decreases for the remainder of the 35-minute measurement in both animals, although in the animal with larger oscillations,

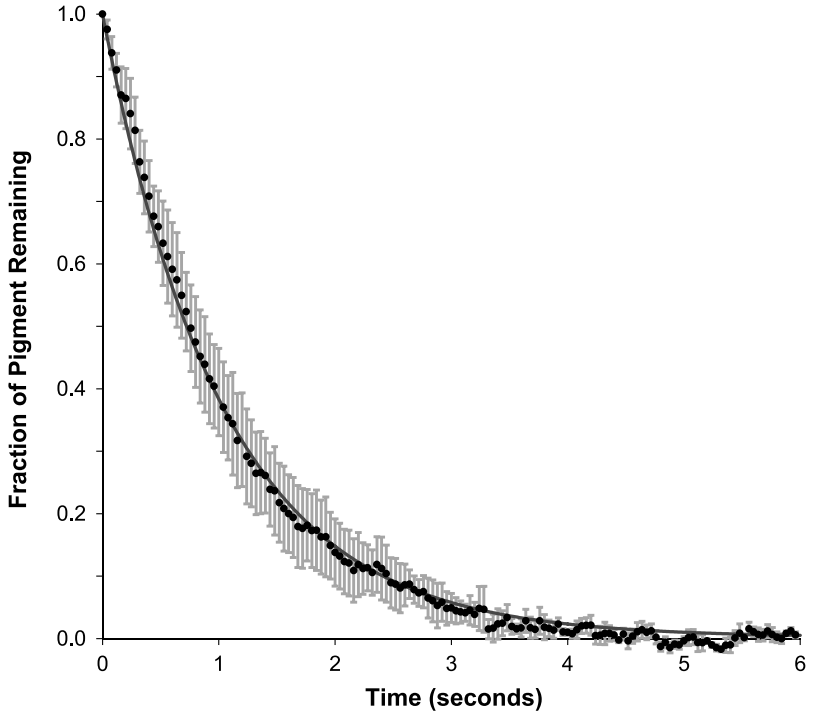

FIGURE 1. The mean of four pigment bleaching experiments at four different locations in animal 1. *Closed circles* are average pixel intensity measured over a 2-degree field of view, normalized to the average intensity measured between seconds 4 and 6. *Error bars*: SEM. The *solid line* is a best-fit plot of equation (1), where $Q/Q_e = 1.01t$.

the reflectance decreases below the baseline value a second time. The reflectance beyond 35 minutes is unknown.

In one location in animal 1, spatial segregation of the 794-nm reflectance signal recorded from rods and cones, which are distinguishable in AOSLO images, was performed. The cones occupied approximately 16% of the retinal area in the imaged location. Reflectance analysis shows similar time courses for rod and cone reflectance with only minor amplitude differences (Fig. 4).

Comparison of Normalization Methods

Figure 5 shows an average of all bleach and recovery data normalized using each of the three methods (infrared, spatial,

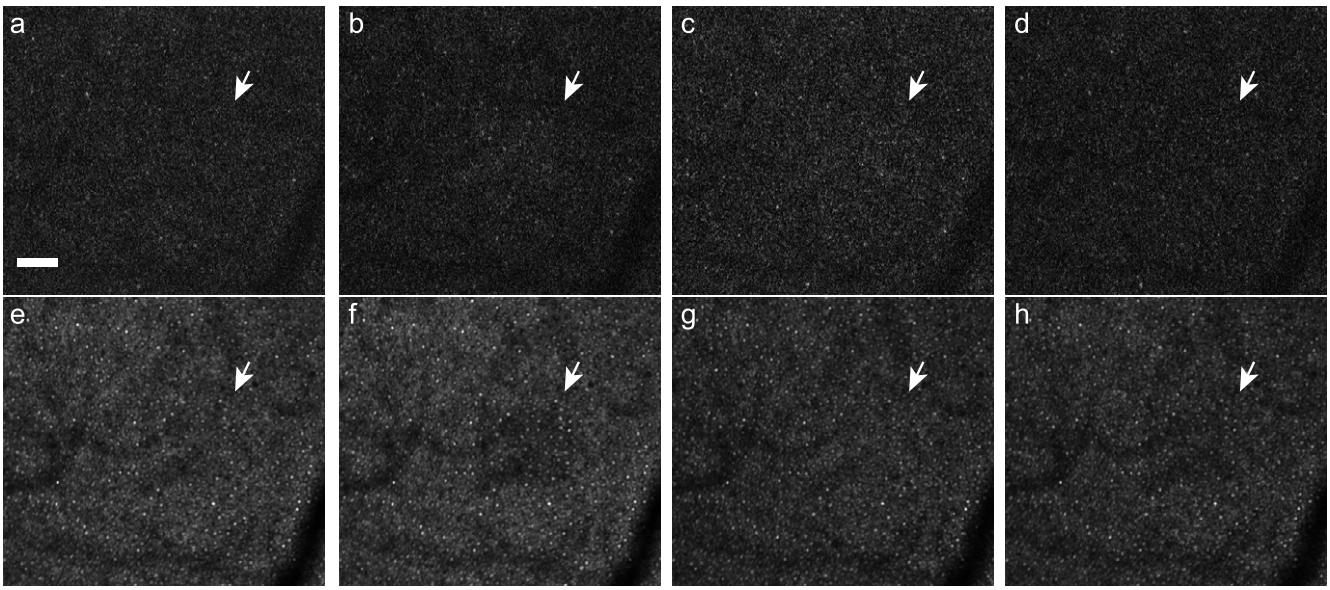

FIGURE 2. Representative reflectance images captured during a densitometry experiment. (**A**–**D**) show 514-nm reflectance and (**E**–**H**) show 794-nm reflectance. The images were recorded immediately before (**A**, **E**), immediately after (**B**, **F**), 7.5 minutes after (**C**, **G**), and 35 minutes after (**D**, **H**) a rhodopsin bleach. The upper right corner of the rectangular area bleached is denoted by *white arrows*. Reflectance from this area at 514 nm increases immediately after the bleach and then slowly recovers to match the surrounding dark-adapted area by 35 minutes. At 794 nm, the reflectance in the bleached area decreases immediately after the bleach, then increases above the surrounding reflectance at 7.5 minutes after the bleach. At 35 minutes, the reflectance has decreased below the surround once more. *Scale bar*: 50 μm.

Investigative Ophthalmology & Visual Science

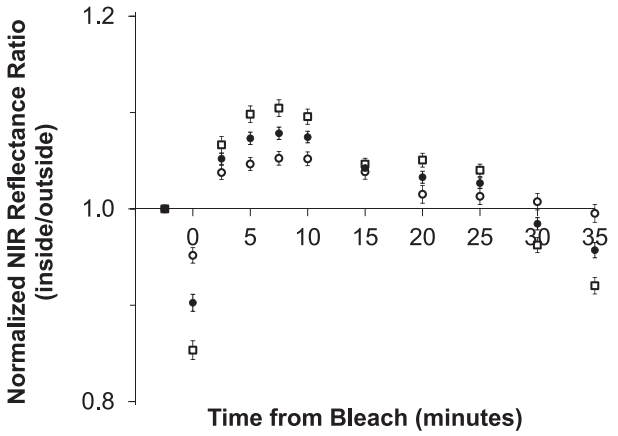

FIGURE 3. Relative NIR (794 nm) reflectance (inside/outside bleach area) captured during rhodopsin density measurements. Values were normalized to the prebleach condition. Each *black circle* is the average of 64 measurements in 16 retinal locations (8 in each animal). The *open circles* are the average of the 32 measurements from animal 1 and the *open squares* are the average of those from animal 2. Both monkeys show a significant drop in reflectance immediately after the bleach, which recovers and increases beyond the prebleach value before decreasing again over the course of 30 minutes. The amplitude of the reflectance fluctuations in animal 1 is significantly larger than that in animal 2 ($P < 0.001$). *Error bars*: SEM.

and combined). Both the infrared and the combined normalization inevitably show features that are related to the infrared oscillations, which cannot be caused by photopigment absorptance. These curves do not conform to what we know about the behavior of regenerating pigment. As just one example, the combined normalization method yields a curve that falls below the baseline, rising again thereafter.

Apparent Density and Recovery Rates

The spatial normalization generated a rhodopsin regeneration time course most like that predicted by the rate-limited model,[29] and was used to compute apparent density and the rate of recovery. The power used for bleaching varied somewhat from 11 μW to 25 μW at the cornea according to the maximum throughput of the AOM on a particular day. Thus, the scotopic energy density of the 2-second bleaching exposures ranged from 3.6×10^7 scot Td·s to 8.4×10^7 scot Td·s (this assumes no loss through ocular media). The effective bleach produced by these energy densities was between 84% and 99% of available rhodopsin.

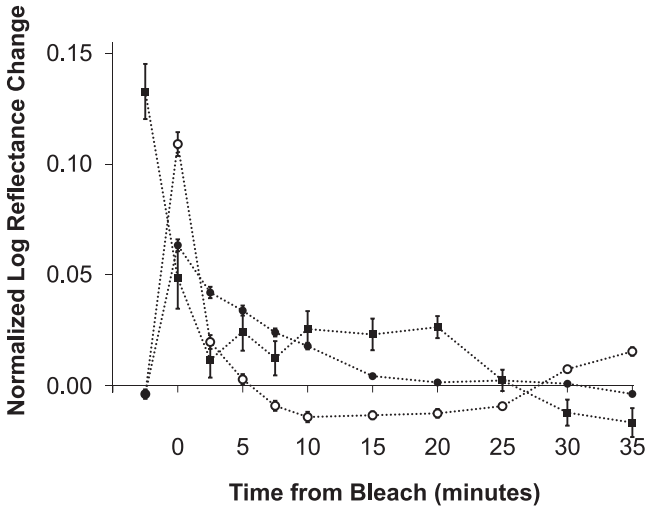

FIGURE 5. Average apparent density as a function of time from the 514-nm bleach, calculated using infrared (*filled squares*), spatial (*filled circles*), and combined infrared and spatial (*open circles*) normalization. The infrared normalization shows evidence of reflectance fluctuations that are likely within the imaging system. These fluctuations are removed by combining infrared with spatial normalization, but the resulting combined curve is clearly corrupted by fluctuations in 794-nm reflectance (see Fig. 3). The spatial normalization generates a time course that is most similar to previously reported rhodopsin kinetics. All data points are the average of 64 bleaches in 16 retinal locations (8 in each animal). *Error bars*: SEM.

In the single location tested, removal of cone reflectance (via masking) before fitting the rhodopsin regeneration time course had no significant effect on the measured apparent density or initial recovery rate ($P = 0.14$ and $P = 0.19$, respectively). Figure 6 shows a comparison of these values determined with and without including cone reflectance. The

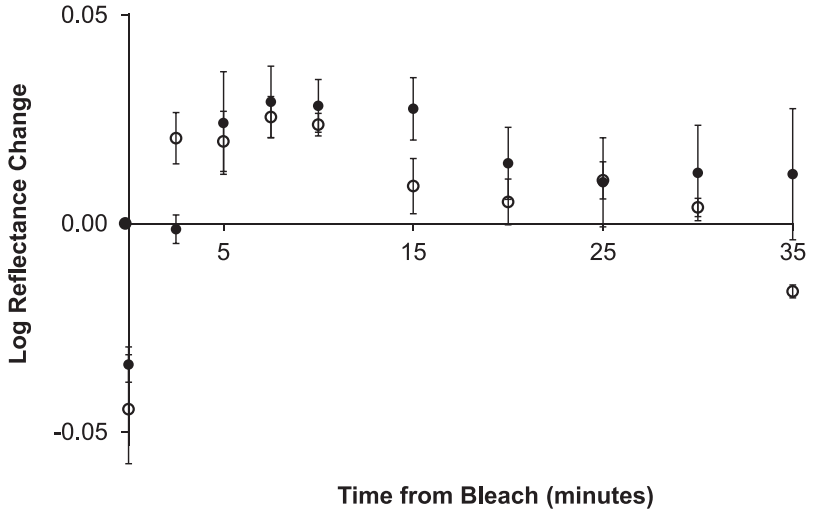

FIGURE 4. Reflectance of the cone (*filled circles*) and rod (*open circles*) photoreceptors measured at 794 nm as a function of time from a full rhodopsin bleach at 514 nm. Both rods and cones show a significant drop in reflectance immediately after the bleach, which recovers and increases beyond the prebleach value before decreasing again over the course of 30 minutes. Data shown are the average of four bleach and recovery measurements in one location in animal 1. *Error bars*: SEM.

Investigative Ophthalmology & Visual Science

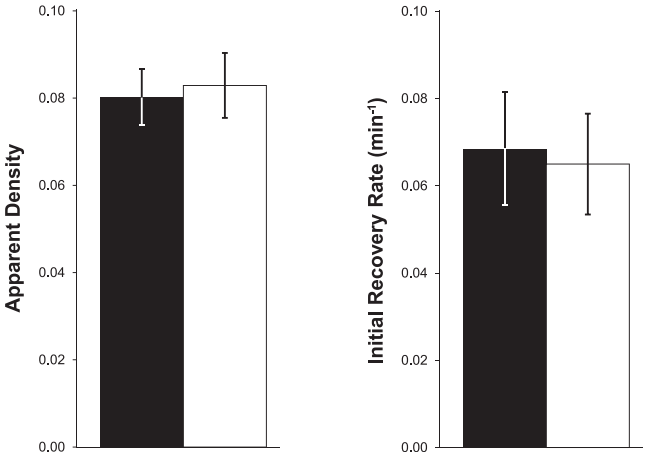

Figure 6. Average apparent density and initial recovery rate calculated by fitting data from four rhodopsin recovery measurements in one retinal location in animal 1, with and without masking of the cone contribution. The *black bars* represent measurements that included cone reflectance, and *white bars* represent measurements made with the cones masked. The average apparent densities and recovery rates measured were not significantly different ($P = 0.14$ and $P = 0.19$, respectively). *Error bars*: SEM.

measured apparent densities were 0.080 ± 0.006 and 0.083 ± 0.007, and the initial recovery rates were 0.069 ± 0.013 min^{-1} and 0.065 ± 0.012 min^{-1}, determined with and without cone reflectance, respectively. This is not surprising given a number of factors that conspire to reduce the relative impact of cones in peripheral retina: the area occupied by cones in the peripheral retina is small (16% in the case we examined), the collection area of cones may be smaller still, and the length of cone outer segments outside the fovea is smaller than that of rods.[31–33] All other densitometric measurements here reported were made without removing cone reflectance.

Figure 7 shows a least-squares fit to the average of all spatially normalized data, which was used to determine the value of K_m (Equation 9) to be 0.2, the value used in the fits for each location. Mean apparent density and recovery rate for each of the 16 retinal locations measured is shown in Table 2. An average of all the best-fit values gives significantly different apparent densities of 0.073 ± 0.006 for animal 1 and 0.032 ± 0.003 for animal 2 ($P = 9.7 \times 10^{-6}$). Average initial recovery rates for these animals were not significantly different ($P = 0.67$); 0.064 ± 0.005 min^{-1} and 0.069 ± 0.004 min^{-1}, respectively.

Table 2. Best Values for mean Apparent Density ($D_{apparent}$) and Initial Recovery Rate (v) From Weighted, Least-Squares Fitting of Densitometry Measurements From Each Location Tested

Animal	Location	$D_{apparent}$	v, min^{-1}
1	A	0.084	0.084
1	B	0.075	0.074
1	C	0.100	0.066
1	D	0.086	0.079
1	E	0.045	0.041
1	F	0.067	0.061
1	G	0.064	0.048
1	H	0.065	0.062
2	A	0.033	0.058
2	B	0.023	0.070
2	C	0.022	0.082
2	D	0.034	0.080
2	E	0.047	0.080
2	F	0.044	0.066
2	G	0.028	0.062
2	H	0.025	0.051

All locations were 15° from the fovea.

Discussion

Origin of Retinal Reflectance Changes That Cannot Be Attributed to Photopigment Absorptance

Our measurements show fluctuations in NIR reflectance that were related to the bleaching exposure but could not have been caused by photopigment absorption. The existence of

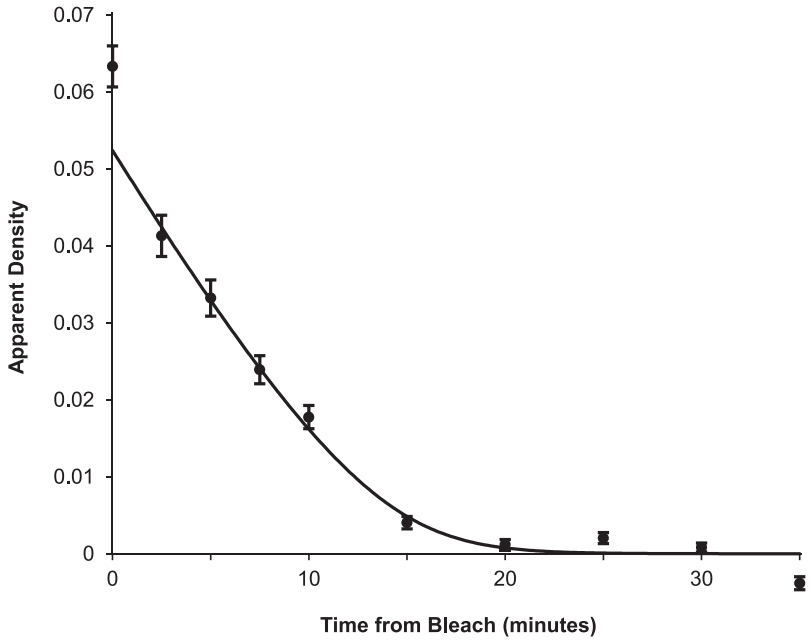

Figure 7. Plot showing the mean of all spatially normalized data ($n = 64$). The *solid line* is the rate-limited kinetics model with $B = 0.94$, $D_{apparent} = 0.056$, $v = 0.074$ min^{-1}, and $K_m = 0.2$. The $t = 0$ time point was excluded from the fit.

such changes is no surprise; stimulus-driven fluctuations of NIR reflectance are commonly observed throughout the nervous system.[34] In the retina, NIR reflectance changes have been measured at a number of time scales. Tsunoda et al.[34] reported four different types of such intrinsic reflectance signals whose time course lasted from seconds to minutes, depending on the stimulus delivered and the retinal area of interest. Pepperberg et al.[35] demonstrated NIR scattering changes on the order of seconds in ex vivo bovine photoreceptors in response to visible light. Also, Schallek et al.[36,37] were able to localize rapid reflectance changes (occurring less than 5 seconds after a stimulus) measured in cat retina to outer retinal layers using pharmacological perturbations.

Looking at effects on the order of seconds, Grieve and Roorda[38] used an AOSLO to demonstrate that the reflectance of human cone photoreceptors at 840 nm showed fluctuations when stimulated with brief flashes at 658 nm. Using an SLO adapted for photopigment densitometry, DeLint et al.[18] measured reflectance changes with a much longer time course, on the order of 30 minutes. The source of these photoreceptor reflectance fluctuations is thought to be a change in the refractive index difference between the photoreceptors and their milieu. For example, exposure to light induces significant movement of phototransduction-associated proteins (e.g., transducin and arrestin) between the inner and outer segments.[39,40] Such changes in protein concentration occur over tens of minutes and are likely involved, but a quantitative model relating protein concentration changes and photoreceptor reflectance has yet to be developed.

Comparison With DeLint et al.

Both the present study and DeLint et al.[18] demonstrate significant changes in retinal reflectance that cannot be attributed to photopigment. They found no evidence of nonphotopigment reflectance changes from the rods, noting a lack of effect at 794 nm in the periphery (beyond 6° from the fovea). Our ability to spatially distinguish the rod and cone mosaics allowed us to determine that these reflectance changes occur in rods as well as cone photoreceptors in the peripheral retina. The time course of the changes reported by DeLint et al.[18] was somewhat different than we observed. They measured a continuous reduction of 740-nm reflectance after their light-adapting source was extinguished, which proceeded for approximately 5 minutes before reaching its lowest value and then recovered to the dark-adapted condition over the course of another 30 minutes. The differences between our findings and theirs may stem from the difference in the duration of bleaching, which was 15 minutes in the study by DeLint et al.[18] and 2 seconds in our study.

Implications of Nonphotopigment Changes for Retinal Densitometry

Despite these differences, both the present study and the study by DeLint et al.[18] demonstrate an important complication in the interpretation of retinal densitometry. Simultaneous red or NIR reflectance measurements often have been used as a means of rejecting fluctuations in the signal obtained by a densitometer that are not related to pigment density.[3,4,6–8,14] The assumption underlying the infrared and combined normalization methods (i.e., that the reflectivity of the retina at 794 nm is constant) is incorrect. We found variations in reflectance not related to photopigment of up to 9%, which approaches half of the 20% change we typically saw in visible light reflectance that would normally be used in retinal densitometry to compute pigment density. The spatial normalization method has the advantage that it uses the reflectance of retina that has not been bleached as a reference. This method is an alternative way to remove fluctuations such as those intrinsic to the light source, imaging system, or the eye's optics. Indeed, we found that spatial normalization greatly reduced the variability of reflectance measurements. However, reflectance changes not related to pigment that occur in the bleached retinal area can still contaminate the estimate of pigment density, even if infrared normalization is avoided. Indeed, DeLint et al.[18] argued that changes not caused by photopigment absorptance occur at a variety of visible wavelengths, including the 514 nm used in this study, as well as the NIR.

Apparent Density and Rate of Recovery

We had anticipated that retinal densitometry in a confocal AOSLO would produce higher estimates of apparent pigment density than previous retinal densitometers because of its increased axial resolution, which rejects stray light from planes other than the receptors. Surprisingly, we found lower estimates of density than most previous studies. The two animals tested in this study showed significantly different average apparent rhodopsin densities. The mean apparent density measured in animal 1 (0.073 ± 0.006) was consistent with previous measurements in macaques and humans. However, animal 2 in our study showed an average apparent density of 0.032 ± 0.003, well below those reported in previous studies. It may be that the animal selected happened to have relatively low pigment density. Kremers and van Norren,[41] for example, reported an uncorrected rhodopsin density in macaques of 0.09 using a similar method. Also, Morgan and Pugh[14] recently published fundus reflectance measurements after rhodopsin bleaching in humans. They reported normalized reflectance changes in 12 subjects ranging from 0.14 to 0.48. These numbers are equivalent to apparent densities ranging from 0.06 to 0.17. However, even these higher values are low compared with ex vivo measurements.

Abundant evidence has shown that the specific density of rhodopsin in primate and human rods is 0.016 to 0.018 OD/μm,[42,43] so the total axial absorbance for a single pass through a 25-μm rod outer segment would be 0.40 to 0.45, far below the apparent axial absorbance of rods that we have measured, and that measured in other retinal densitometry studies.[14,41] Thus, our results further confirm that reflection densitometry cannot be used to directly measure the true axial absorbance of visual pigments. Clearly, physical models of light propagation through and reflection by ocular tissues that incorporate all changes in reflectance accompanying bleaching are needed to understand our results. The ineffectiveness of confocal AOSLO imaging in increasing the apparent photopigment density suggests that most of the stray light that dilutes the density estimate arises from layers within the axial resolution of the AOSLO, which we estimate to be approximately 60 μm. A major source is likely to be within the receptor itself, at the junction between the cone inner and outer segment, as revealed by optical coherence tomography.[44,45]

The question arises, however, why our measurements with an AOSLO yield lower apparent densities than those obtained by others using instruments without adaptive optics. One possibility is that the infrared normalization used in previous studies overestimates the density, as DeLint et al.[18] reported. A second possibility is that our use of an unusually large entrance pupil decreased the fraction of returning light that passed through photopigment. Given the breadth of the Stiles-Crawford effect for rods, this would be surprising, but we have not undertaken any experiments to directly address this

question. It also may be the case that our protocol for anesthesia and paralysis affected the retinoid cycle in these animals. Lamb and Pugh[46] noted that certain anesthetics, such as ketamine (which was used during transportation and preexperimental setup), can reduce the rate of rhodopsin regeneration or stop the retinoid cycle entirely. But, it is likely that the effect of these drugs would have dissipated before the density measurements were taken. It also should be noted that the initial recovery rates measured in these two animals (0.064 $\pm$ 0.005 min^{-1} and 0.069 $\pm$ 0.004 min^{-1}, respectively) were slightly lower than what has been reported previously in human eyes (0.073 min^{-1} and 0.090 min^{-1} from Morgan and Pugh,[14] 0.085 min^{-1} and 0.095 min^{-1} from Lamb and Pugh,[46] 0.146 from van Norren and van de Kraats[47]).

Conclusions

Even various assumptions used in retinal densitometry to extract the apparent density need to be carefully evaluated, including the use of NIR light as a reference beam, the aperture of the illumination system, and the potential for anesthesia to affect photopigment kinetics in animal models. As DeLint et al.[18] pointed out, a change in photopigment density is not the only factor contributing to measured reflectance changes after a bleaching exposure. All present data suggest that photopigment density is the largest contributor to changes in visible reflectance, but NIR measurements demonstrate an additional source of stimulus-dependent variability. Our data show that, even at rod-dominated eccentricities, normalizing density measurements to 794-nm reflectance would result in an overestimate of photopigment density and an increase in the apparent rate of recovery. Future investigations of photopigment kinetics will need to develop a more complex model to account for these fluctuations as well as potential changes in inner retinal and anterior transmissivity, which are likely occurring as well.

These difficulties in the interpretation of retinal densitometry do not negate the utility of this method as a measure of outer retinal function. Although the absolute measurement of pigment density and recovery may be biased by these additional outer retinal reflectance fluctuations, it appears that these fluctuations are related to the bleaching stimulus and thus are themselves indicative of retinal function. Therefore, rhodopsin densitometry with an AOSLO focused on the photoreceptor layer could provide a valuable measure of the functional integrity of the photoreceptor/RPE complex, even though the reflectance changes arise from multiple sources.

Acknowledgments

The authors thank Lee Anne Schery, Jesse Schallek, Lu Yin, Jessica Morgan, Ethan A. Rossi, and William S. Fischer for their assistance.

Supported by the National Institutes of Health, Bethesda, Maryland, through Grants BRP-EY014375, R01-EY022371, R01-EY004367, K23-EY016700, P30-EY001319, and T32-EY07125. The image registration software used to produce our AOSLO images, DeMotion, was developed by Alfredo Dubra and Zach Harvey with funding from Research to Prevent Blindness and the National Institutes of Health through Grants BRP-EY014375 and 5 K23 EY016700. Alfredo Dubra and Kamran Ahmad developed the adaptive optics control software.

Disclosure: **B.D. Masella**, Canon, Inc. (F); **J.J. Hunter**, Polgenix, Inc. (F), Canon, Inc. (F), P; **D.R. Williams**, Polgenix, Inc. (F), Canon, Inc. (F), Pfizer (C, R), P

References

1. Brindley GS, Willmer EN. The reflexion of light from the macular and peripheral fundus oculi in man. *J Physiol*. 1952; 116:350–356.
2. Brindley GS, Rushton WAH. Detection of visual pigment in living human cones. *J Physiol*. 1955;130:59P.
3. Campbell FW, Rushton WA. Measurement of the scotopic pigment in the living human eye. *J Physiol*. 1955;130:131–147.
4. Rushton WA. A cone pigment in the protanope. *J Physiol*. 1963;168:345–349.
5. Rushton WA. The density of chlorolabe in the foveal cones of the protanope. *J Physiol*. 1963;168:360–373.
6. Alpern M. Rhodopsin kinetics in the human eye. *J Physiol*. 1971;217:447–471.
7. Hood C, Rushton WA. The Florida retinal densitometer. *J Physiol*. 1971;217:213–229.
8. van Norren D, van de Kraats J. A continuously recording retinal densitometer. *Vision Res*. 1981;21:897–905.
9. van Norren D, van de Kraats J. Imaging retinal densitometry with a confocal scanning laser ophthalmoscope. *Vision Res*. 1989;29:1825–1830.
10. Elsner AE, Burns SA, Webb RH. Mapping cone photopigment optical density. *J Opt Soc Am A*. 1993;10:52–58.
11. Tornow RP, Beuel S, Zrenner E. Modifying a Rodenstock scanning laser ophthalmoscope for imaging densitometry. *Appl Opt*. 1997;36:5621–5629.
12. Faulkner DJ, Kemp CM. Human rhodopsin measurement using a t.v.-based imaging fundus reflectometer. *Vision Res*. 1984;24: 221–231.
13. Elsner A, Moraes L, Beausencourt E, et al. Scanning laser reflectometry of retinal and subretinal tissues. *Opt Express*. 2000;6:243–250.
14. Morgan JI, Pugh EN Jr. Scanning laser ophthalmoscope measurement of local fundus reflectance and autofluorescence changes arising from rhodopsin bleaching and regeneration. *Invest Ophthalmol Vis Sci*. 2013;54:2048–2059.
15. Roorda A, Williams DR. The arrangement of the three cone classes in the living human eye. *Nature*. 1999;397:520–522.
16. Rushton WA. Stray light and the measurement of mixed pigments in the retina. *J Physiol*. 1965;176:46–55.
17. King-Smith PE. The optical density of erythrolabe determined by retinal densitometry using the self-screening method. *J Physiol*. 1973;230:535–549.
18. DeLint PJ, Berendschot TT, van de Kraats J, van Norren D. Slow optical changes in human photoreceptors induced by light. *Invest Ophthalmol Vis Sci*. 2000;41:282–289.
19. Bedggood P, Metha A. Variability in bleach kinetics and amount of photopigment between individual foveal cones. *Invest Ophthalmol Vis Sci*. 2012;53:3673–3681.
20. Gray DC, Merigan W, Gee BP, et al. In vivo high-resolution fluorescence retinal imaging with adaptive optics. Presented at: Frontiers in Optics; October 10, 2006; Rochester, NY.
21. Hunter JJ, Masella B, Dubra A, et al. Images of photoreceptors in living primate eyes using adaptive optics two-photon ophthalmoscopy. *Biomed Opt Express*. 2010;2:139–148.
22. Lamb TD, Pugh EN Jr. Dark adaptation and the retinoid cycle of vision. *Prog Retin Eye Res*. 2004;23:307–380.
23. Gray DC, Merigan W, Wolfing JI, et al. In vivo fluorescence imaging of primate retinal ganglion cells and retinal pigment epithelial cells. *Opt Express*. 2006;14:7144–7158.
24. Morgan JI, Hunter JJ, Masella B, et al. Light-induced retinal changes observed with high-resolution autofluorescence imaging of the retinal pigment epithelium. *Invest Ophthalmol Vis Sci*. 2008;49:3715–3729.

25. Morgan JI, Dubra A, Wolfe R, Merigan WH, Williams DR. In vivo autofluorescence imaging of the human and macaque retinal pigment epithelial cell mosaic. *Invest Ophthalmol Vis Sci*. 2009;50:1350–1359.
26. Dubra A, Harvey Z. Registration of 2D images from fast scanning ophthalmic instruments. *Lect Notes Comput Sci*. 2010;6204:60–71.
27. van de Kraats J, Berendschot TTJM, van Norren D. The pathways of light measured in fundus reflectometry. *Vision Res*. 1996;36:2229–2247.
28. Venkateswaran K, Roorda A, Romero-Borja F. Theoretical modeling and evaluation of the axial resolution of the adaptive optics scanning laser ophthalmoscope. *J Biomed Opt*. 2004;9:132–138.
29. Mahroo OA, Lamb TD. Recovery of the human photopic electroretinogram after bleaching exposures: estimation of pigment regeneration kinetics. *J Physiol*. 2004;554:417–437.
30. Michaelis L, Menten ML. Die Kinetik der Invertinwirkung. *Biochem Z*. 1913;49:333–369.
31. Krebs W, Krebs IP. Quantitative morphology of the primate peripheral retina (*Macaca irus*). *Am J Anat*. 1987;179:198–208.
32. Curcio CA, Sloan KR, Kalina RE, Hendrickson AE. Human photoreceptor topography. *J Comp Neurol*. 1990;292:497–523.
33. Spaide RF, Curcio CA. Anatomical correlates to the bands seen in the outer retina by optical coherence tomography: literature review and model. *Retina*. 2011;31:1609–1619.
34. Tsunoda K, Hanazono G, Inomata K, Kazato Y, Suzuki W, Tanifuji M. Origins of retinal intrinsic signals: a series of experiments on retinas of macaque monkeys. *Jpn J Ophthalmol*. 2009;53:297–314.
35. Pepperberg DR, Kahlert M, Krause A, Hofmann KP. Photic modulation of a highly sensitive, near-infrared light-scattering signal recorded from intact retinal photoreceptors. *Proc Natl Acad Sci U S A*. 1988;85:5531–5535.
36. Schallek J, Kardon R, Kwon Y, Abramoff M, Soliz P, Tso D. Stimulus-evoked intrinsic optical signals in the retina: pharmacologic dissection reveals outer retinal origins. *Invest Ophthalmol Vis Sci*. 2009;50:4873–4880.
37. Schallek J, Li H, Kardon R, et al. Stimulus-evoked intrinsic optical signals in the retina: spatial and temporal characteristics. *Invest Ophthalmol Vis Sci*. 2009;50:4865–4872.
38. Grieve K, Roorda A. Intrinsic signals from human cone photoreceptors. *Invest Ophthalmol Vis Sci*. 2008;49:713–719.
39. Sokolov M, Lyubarsky AL, Strissel KJ, et al. Massive light-driven translocation of transducin between the two major compartments of rod cells: a novel mechanism of light adaptation. *Neuron*. 2002;34:95–106.
40. Calvert PD, Strissel KJ, Schiesser WE, Pugh EN Jr, Arshavsky VY. Light-driven translocation of signaling proteins in vertebrate photoreceptors. *Trends Cell Biol*. 2006;16:560–568.
41. Kremers JJ, van Norren D. Retinal damage in macaque after white light exposures lasting ten minutes to twelve hours. *Invest Ophthalmol Vis Sci*. 1989;30:1032–1040.
42. Baylor DA, Nunn BJ, Schnapf JL. The photocurrent, noise and spectral sensitivity of rods of the monkey *Macaca fascicularis*. *J Physiol*. 1984;357:575–607.
43. Dartnall HJ, Bowmaker JK, Mollon JD. Human visual pigments: microspectrophotometric results from the eyes of seven persons. *Proc R Soc Lond B Biol Sci*. 1983;220:115–130.
44. Jonnal RS, Rha J, Zhang Y, Cense B, Gao WH, Miller DT. In vivo functional imaging of human cone photoreceptors. *Optics Express*. 2007;15:16141–16160.
45. Jonnal RS, Kocaoglu OP, Wang Q, Lee S, Miller DT. Phase-sensitive imaging of the outer retina using optical coherence tomography and adaptive optics. *Biomed Opt Express*. 2012;3:104–124.
46. Lamb TD, Pugh EN Jr. Phototransduction, dark adaptation, and rhodopsin regeneration the proctor lecture. *Invest Ophthalmol Vis Sci*. 2006;47:5137–5152.
47. van Norren D, van de Kraats J. Retinal densitometer with the size of a fundus camera. *Vision Res*. 1988;29:369–374.

Investigative Ophthalmology & Visual Science